

Check for updates







High Impedance Mudstone Associated With Sand Injection Complexes: Significance for Basin-Scale Fluid Retention and Escape

Rene Jonk^{1,2} 🕞 | Marnix Vermaas³ | Bader Al-Aamri^{1,4} | Tara L. Stephens^{1,5}

 1 Department of Geology & Geophysics, School of Geosciences, University of Aberdeen, Aberdeen, UK | 2 ACT-Geo Ltd., Geoscience Consulting and Training, Aberdeen, UK | 3 Apache Corporation, Houston, Texas, USA | 4 Petroleum Development Oman, Muscat, Oman | 5 British Geological Survey, Lyell Centre, Edinburgh, UK

Correspondence: Rene Jonk (rene.jonk@abdn.ac.uk)

Received: 8 January 2025 | Revised: 20 June 2025 | Accepted: 3 August 2025

Funding: The authors received no specific funding for this work.

Keywords: acoustic impedance | mudstones | overpressure | sand injectites | seismic attributes | shale dewatering

ABSTRACT

High impedance (hard) mudstones are sometimes observed in association with sand injection complexes in the Paleogene petroleum province of the northern North Sea. A hard mudstone surrounding a water-bearing sandstone can give a similar acoustic response to an oil-bearing sandstone surrounded by low impedance (soft) mudstone. The presence of hard mudstone thus impacts the ability to predict hydrocarbon presence directly from seismic data during exploration. To establish the mechanism of 'hardening' to better predict the presence of variable mudstone characteristics, we examine three cored wells from the Beryl Embayment. Well logs and core were examined to characterise the structure, petrology, petrophysical properties and spatial distribution of both hard and soft mudstones. The results indicate that mudstone hardening is most likely associated with mechanical compaction and efficient dewatering of mudstones into the sand injection complex. This process is enhanced where sand injection complexes transect primary overpressure zones, that promote dewatering from basal overpressured mudstone into the injection network. This study highlights that seismic response needs careful investigation in the context of the complexity of the injectite complex along with variable mudstone attributes. Additionally, this process highlights the role sand injection complexes play in efficient dewatering through lateral transfer in overpressured basins.

1 | Introduction

Seismic-based exploration for hydrocarbons is greatly enhanced by using direct hydrocarbon indicators, including flat spots, amplitude-conformance to structure and rock-property-calibrated amplitude variation with angle offset (AVO; Simm 2017). In some stratigraphic trap configurations, identification of confident flat spots and amplitude-conformance is ambiguous, and seismic-based derisking of hydrocarbon fluid presence relies heavily on the AVO response alone (Castagna et al. 1998). This is commonly the case for sand injection

complexes in the Paleogene deep-water depositional province of the northern North Sea (Hurst et al. 2003; Huuse et al. 2004; Pernin et al. 2022), where the reservoir and fluid configuration primarily rely on identifying AVO response. The seismic reflectivity response as a function of angle offset of an interface or tuned reservoir interval is a function of both the reservoir and adjacent seal lithology. Thus, discrimination of whether a response can be tied to the fluid type present in the reservoir, it is critical to model the appropriate rock physics response of the reservoir and seal lithologies. Typically, reservoir properties are the focus of such AVO calibration workflows. However,

This is an open access article under the terms of the Creative Commons Attribution License, which permits use, distribution and reproduction in any medium, provided the original work is properly cited.

© 2025 The Author(s). Basin Research published by International Association of Sedimentologists and European Association of Geoscientists and Engineers and John Wiley & Sons Ltd.

Summary

- Understanding the acoustic properties of surrounding mudstones aids in the prediction of fluid type in sand injectite reservoirs from seismic data.
- Anomalously high impedance ('hard') mudstones are associated with dewatering through surrounding sand injectites, only in basinal positions where the injection complexes straddle primary (disequilibrium compaction) overpressure zones.
- The three-dimensional complexity of sand injection complexes, along with the complex distribution of primary overpressure, means zones of anomalous shale dewatering are focused towards the base of sand injection complexes that connect vertically to lower pressure regimes.

varied acoustic properties of the surrounding mudstones may in some cases complicate the evaluation (Figure 1). In this study, the observation of highly variable acoustic properties of encasing mudstones (Figure 2) adds to the complexity of fluid type prediction. Appropriate consideration of mudstone physical properties when evaluating fluid response associated with injectite reservoirs needs to be incorporated to enhance our understanding of the origin of these variable mudstone properties and predict the spatial occurrence of high impedance (hard) mudstones. In addition to the direct application for hydrocarbon exploration, this study highlights the importance of large-scale sand injection complexes in controlling short and long-lived fluid flow in sedimentary basins (Jonk 2010). While the process that forms injection complexes is associated with significant fluid flow events (Jonk et al. 2003; Vigorito et al. 2022), the creation of permeable vertical pathways can facilitate long-term transfer of fluids (Jonk, Hurst, et al. 2005;

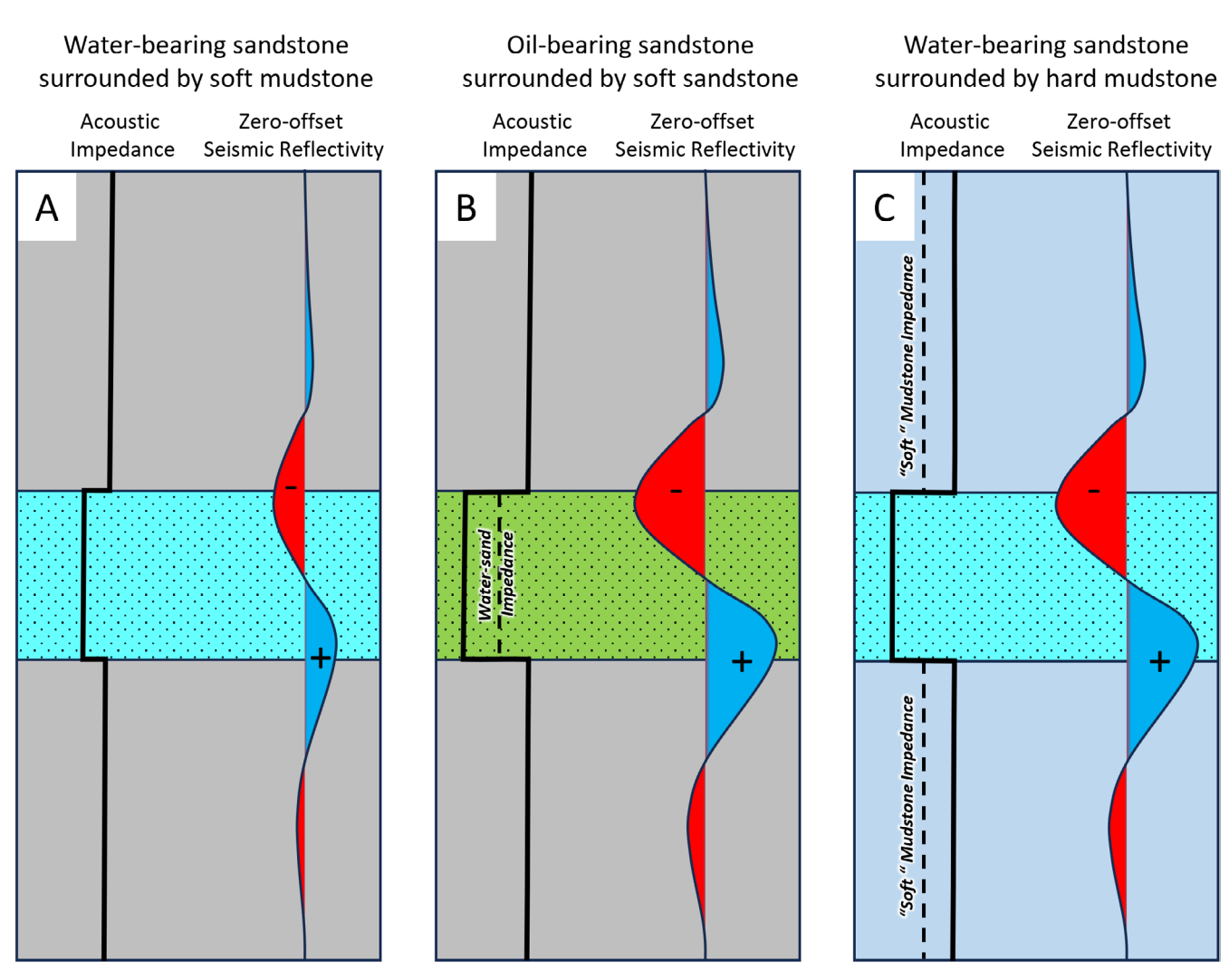


FIGURE 1 | Cartoon illustrating the complexities arising from the variable acoustic properties of encasing mudstone on fluid type prediction from (inverted) seismic reflectivity data. Three cases are shown with an acoustic impedance structure (solid line) and a zero phase zero-offset convolved wavelet response for a perfectly tuned sandstone layer (red denotes decreases in impedance, blue denotes increases in impedance) encased in mudstone with variable properties. (A) Impedance and zero-offset reflectivity response of water-saturated sandstone encased in low impedance mudstones. (B) Impedance and zero-offset reflectivity response of water-saturated sandstone (dashed line shows reference water-sand) encased in low impedance mudstones. (C) Impedance and zero-offset reflectivity response of water-saturated sandstone (dashed line shows reference soft mudstone response) encased in high impedance mudstone.

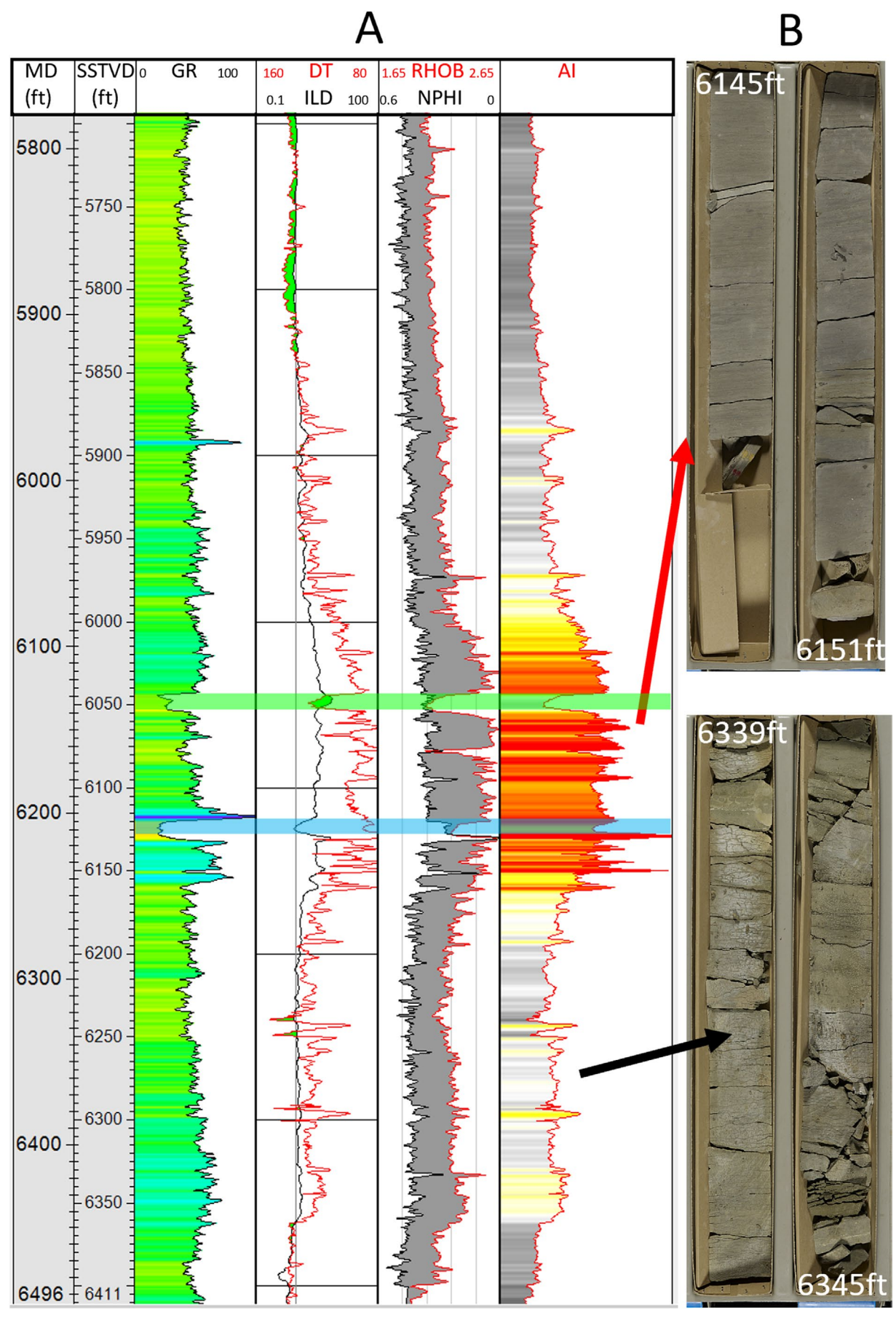


FIGURE 2 | Legend on next page.

FIGURE 2 | (A) Wireline log (9/15-2 well) of sandstone intrusion reservoirs (upper green zone oil bearing, lower blue zone water-bearing) encased in mudstones with significant variability in impedance. (B) core from hard mudstone (top, 1872–1874 m, British Geological Survey Image S00071913) and soft mudstone (base, 1931–1933 m, British Geological Survey Image S00071916). UKRI 2024. Licensed under the Open Government Licence v3.0.

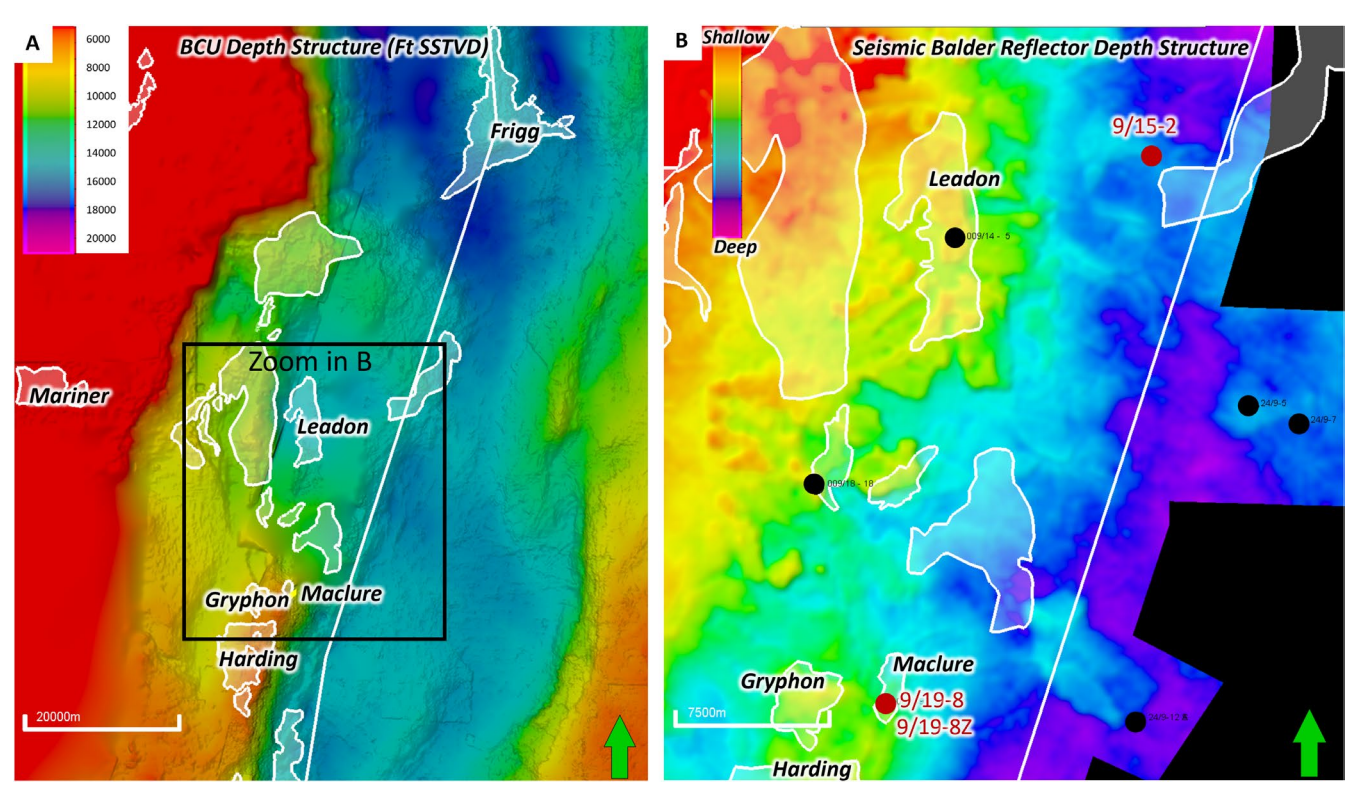


FIGURE 3 | (A) Regional map showing the depth structure on the Base Cretaceous Unconformity (BCU), displaying the tectonic architecture of the Beryl Embayment on the edge of the South Viking Graben. Key hydrocarbon fields hosted in Paleogene clastic reservoirs are highlighted. White line denotes the UK-Norway offshore boundary (B) Zoom-in map of the depth-structure of the Top Balder Seismic Reflector, showing the broad shelf to slope to basin-floor clastic depositional domains associated with some of the key Tertiary hydrocarbon fields. Cored wells studied in this study are shown in red. Other wells investigated are shown in black (see Table 2).

Jonk, Parnell, and Hurst 2005). The interactions of fluids in surrounding low permeability sediments (mudstones) with these permeable sand injection complexes are poorly studied, as are the effects of sand injection complexes on the physical properties of adjacent mudstones.

2 | High Impedance Mudstone Associated With Sand Injection Complexes: Regional Setting and Well Database

The area of focus is the slope-to-basin-floor setting of the Beryl Embayment extending into the South Viking Graben in the Eocene Balder and Frigg Formations (Jones et al. 2003; Jonk, Hurst, et al. 2005). The Beryl Embayment developed as a tectonic-scale fault relay ramp separating the East Shetland Platform from the South Viking Graben and was a focus for shelf-to-slope sandstone-rich depositional systems developing throughout the Paleogene (Ahmadi et al. 2003; Jones et al. 2003). Numerous hydrocarbon fields are present in the Paleogene section of the Beryl embayment

region, including the Harding, Gryphon, Leadon, Maclure, Frigg and Mariner fields (Figure 3; Purvis et al. 2002; Templeton et al. 2002). These reservoirs are all sand injection complexes, each sourced from intensely remobilised parent sandstones that were originally deposited in a deepwater slope-to-basin-floor setting. In most cases, the bulk of the hydrocarbon volumes are within the injected sandstones overlying the remobilised depositional sandstones (Szarawarska et al. 2010).

Three wells (9/15a-2, 9/19-8 and 9/19-8z) were identified in the study area that have cored intervals of variably high and low impedance mudstone hosting large sand injection complexes (Figure 4). Eighteen samples were taken to represent a spread of cored mudstone facies as well as a range of logged impedances (Table 1). In addition to the cored samples, we broadened our investigation to include other wells within the area of the seismically inverted acoustic impedance volume. This enabled calibration of wireline log-based impedance signatures more broadly to enhance the core-derived database (Figure 3; Table 2).

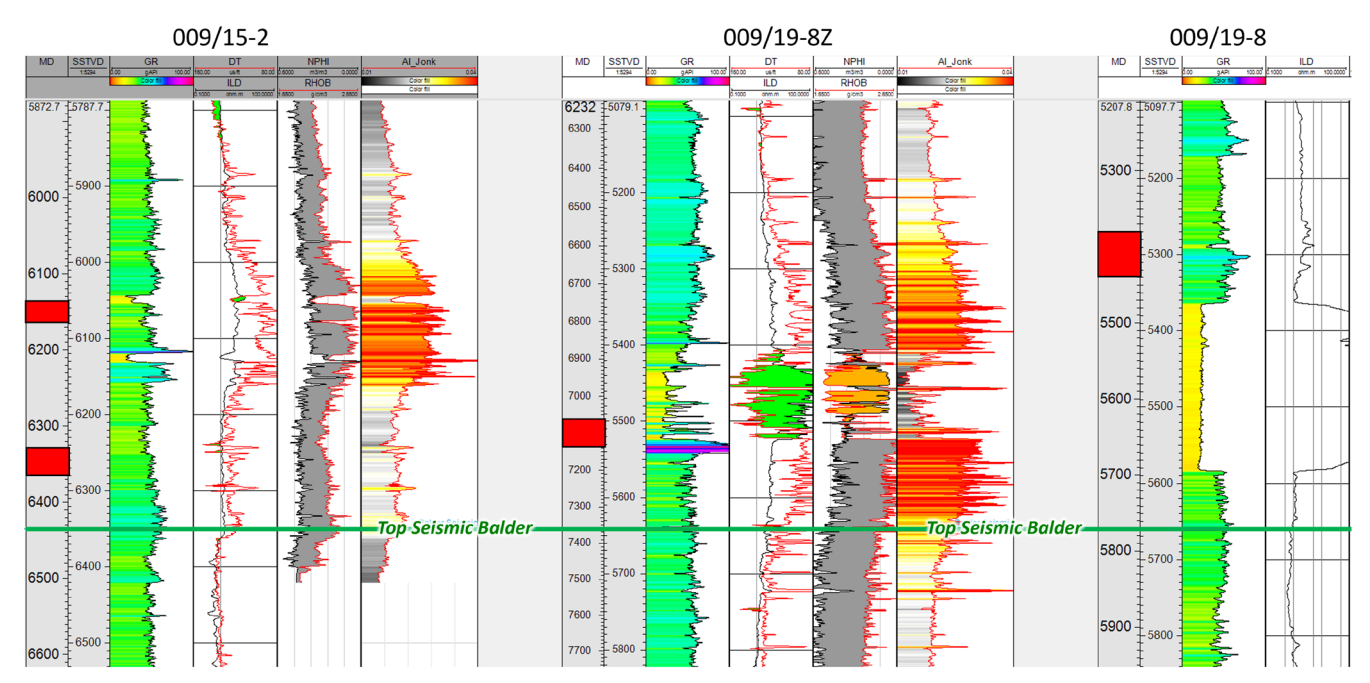


FIGURE 4 | Borehole correlation (flattened on the Top Balder Reflector) of the key wells and cored intervals (red) sampled for mudstone rock properties.

TABLE 1 | Details of the core samples taken.

Well ID	Depth (Ft MD)	BGS sample ID	Lithology	Comments	MICP and thin-section	Portable XRF
9/15a-2	6140	SSK144256	Argillaceous Mudstone	Mudstone interbedded with oil-stained injectites	Х	X
9/15a-2	6149	SSK144257	Argillaceous Mudstone	Laminated Mudstone	X	X
9/15a-2	6155	SSK144258	Calcareous-Argillaceous Mudstone	Laminated Mudstone		X
9/15a-2	6337	SSK144259	Siliceous-Argillaceous-Calcareous Mudstone	Greenish-grey colouring	X	X
9/15a-2	6340	SSK144261	Siliceous-Argillaceous-Calcareous Mudstone	Greenish-grey colouring		X
9/15a-2	6344	SSK144260	Siliceous-Argillaceous-Calcareous Mudstone	Greenish-grey colouring	X	X
9/15a-2	6355	SSK144262	Calcareous-Argillaceous Mudstone	Contains (micro) calcitic fossils	X	X
9/15a-2	6357	SSK144263	Siliceous-Argillaceous-Calcareous Mudstone	Contains reddish (siderite?) nodules		X
9/19-8	5384	SSK144264	Siliceous-Argillaceous-Calcareous Mudstone	Laminated greenish- coloured mudstone		X
9/19-8	5389	SSK144265	Siliceous-Argillaceous-Calcareous Mudstone	Thinly interbedded silty and clayey layers	X	X
9/19-8	5398	SSK144267	Calcite concretion			X
9/19-8	5406	SSK144268	Calcareous-Argillaceous Mudstone	Light-grey colouring	X	X
9/19-8	5431	SSK144269	Siliceous-Argillaceous-Calcareous Mudstone	Contains whitish (calcite?) specks	X	X
9/19-8z	7076	SSK144270	Argillaceous Mudstone	Dark grey colouring	X	X
9/19-8z	7095	SSK144271	Calcareous-Argillaceous Mudstone	Contains whitish (calcite?) laminae		X
9/19-8z	7120	SSK144273	Siliceous-Argillaceous-Calcareous Mudstone	Thinly interbedded silty and clayey layers		X
9/19-8z	7122	SSK144272	Argillaceous Mudstone	Homogenous	X	X
9/19-8z	7127	SSK144274	Siliceous-Argillaceous-Calcareous Mudstone	Thinly interbedded silty and clayey layers		X

Note: Orange are samples from high impedance units, grey are samples from low impedance units. Based upon samples supplied under Loan Number Core286254, British Geological Survey UKRI.

Four hypotheses are postulated to explain the occurrence of high impedance mudstones associated with sand injection complexes (Figure 5).

 Preferential sill-like intrusion along mechanical stratigraphic interfaces. Injectite complexes can contain well defined 'dyke-dominated' and 'sill-dominated' zones (Vigorito and Hurst 2010). Wing-like sandstone intrusions are often observed in both outcrop (Waltham et al. 2025)

TABLE 2 | List of all wells investigated for detailed well log correlation and petrophysical evaluation.

Well ID	Country	Core sampled	Well log suite investigated
9/15a-2	UK	X	GR, NPHI, RHOB, ILD, DTC
9/19-8	UK (Maclure)	X	GR, ILD
9/19-8z	UK (Maclure)	X	GR, NPHI, RHOB, ILD, DTC
24/9-5	Norway		GR, NPHI, RHOB, ILD, DTC
24/9-7	Norway		GR, NPHI, RHOB, ILD, DTC
24/9-3	Norway		GR, NPHI, RHOB, ILD, DTC
9/18-18	UK		GR, NPHI, RHOB, ILD, DTC
9/14-5	UK (Leadon)		GR, NPHI, RHOB, ILD, DTC

- and in the subsurface (Satur and Hurst 2025). Seismic-scale bedding-parallel sand injectites are typically observed at the interface between the Balder and Frigg Formations in the area of study. Differences in acoustic (mechanical) properties are observed within the Balder and Frigg Formations, and particularly along the interface between both formations.
- 2. Anomalous post-intrusion porosity-reducing cementation along intrusion margins. Following their formation, sand injectites form permeable pathways through generally low permeability host strata and can become sites of significant fluid flow focus and associated cementation (Jonk, Hurst, et al. 2005; Jonk, Parnell, and Hurst 2005). Cementation typically takes place at the interface between the sand and the mud and may develop 'hard' cemented intrusion margins.
- 3. Shear-induced deformation (and hardening) of mudstones associated with the injection process. While generally the focus on the formation processes of sand injectites focuses on the formation of the intrusion fractures (Cartwright et al. 2008), coincident brittle and ductile deformation within the surrounding mudstones has not been investigated in detail. Hard margins, including slickensided surfaces, have been described as being associated with some sand injection complexes (Hurst et al. 2025) and may result in the hardening observed.
- 4. Focused post-intrusion dewatering of mudstones into the permeable sandstone intrusions. By their nature, sand injection complexes provide vertical and lateral pathways within and through generally low-permeability host rocks. While the specific role of sand injection complexes in basinal dewatering has not yet been studied in

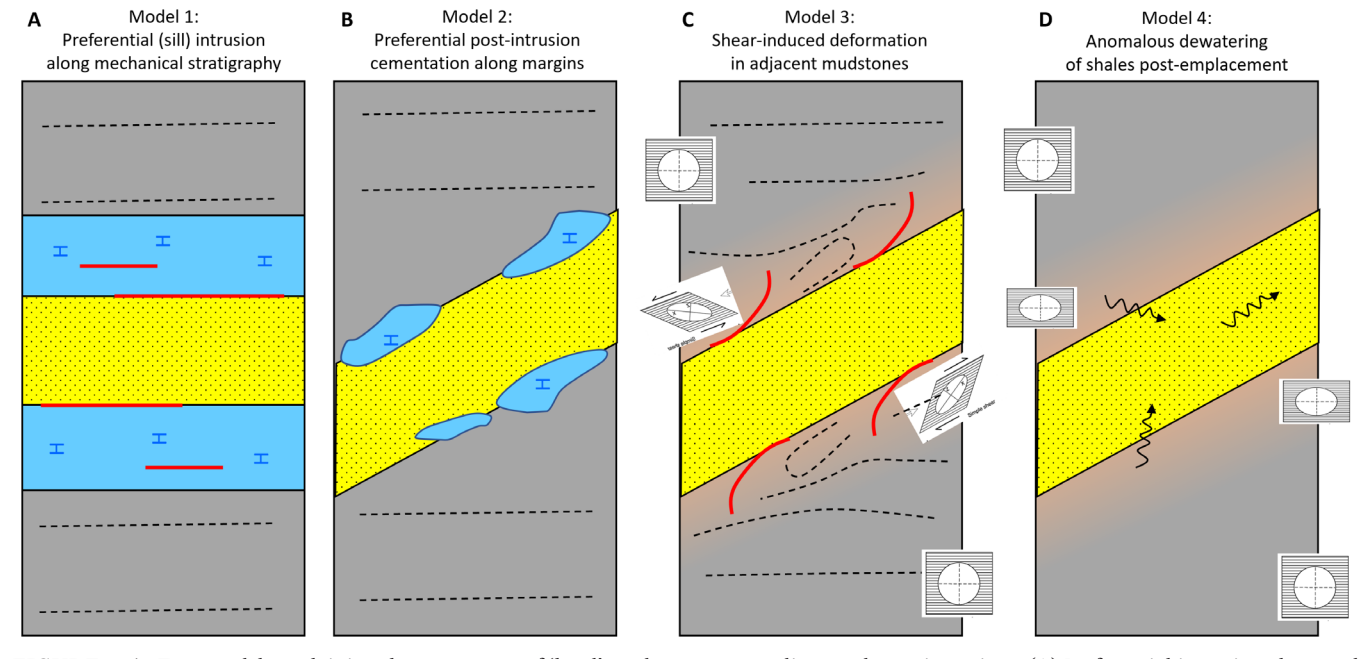


FIGURE 5 | Four models explaining the occurrence of 'hard' mudstone surrounding sandstone intrusions. (A) Preferential intrusion along and within stiff mudstones (blue calcareous mudstones) containing bedding-parallel planes of zero strength (red). (B) Preferential cementation along the margins of intrusions (blue patches). (C) Shear stress increases (associated with drag along intrusion margins) with deformation fabrics (folds, dashed lines, extensional and compressional shear faults, red lines). (D) Pure shear mechanical compaction along the margins associated with dewatering of mudstone.

great detail, the general concept of lateral transfer of fluids through permeable strata is well understood (Yardley and Swarbrick 2000).

For each of these models, we postulate critical rock property and seismic-scale observations that would support or refute the hypothesis. In addition, a critical component of the study

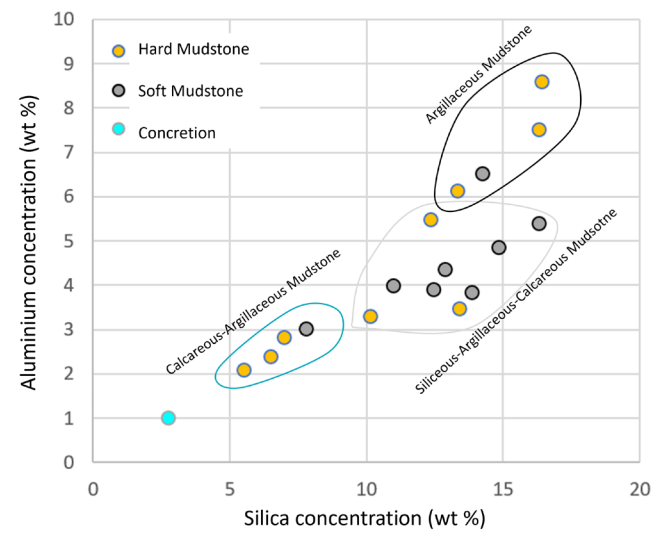


FIGURE 6 | Mineralogical variations (inferred from XRF-derived elemental composition) indicating broadly different mudstone types do not systematically correspond with the harder and softer mudstone intervals observed in the cores.

is to enhance predictability; anomalously high impedance mudstones are spatially restricted, so models should allow for predictability in the absence of core, well log and high-fidelity seismic inversion control.

3 | Mudstone Rock Properties: Core and Wireline Log Observations

Eighteen mudstone samples were taken across both high and low impedance intervals associated with sand injection complexes (Table 1). A hand-lens based description was made for each sample (using the mudstone nomenclature scheme of Milliken 2014). This was accompanied by elemental compositional data acquired using a portable X-Ray Fluorescence (XRF) device (Hou et al. 2004). A subset of 10 samples were selected for more detailed characterisation by thin-section petrography, supplemented by Mercury (Hg) Injection Capillary Pressure (MICP) tests (Davudov et al. 2018; Jonk et al. 2022) to quantify grain density and total Hg porosity (Table 1).

Using the elemental data derived from the XRF analysis, we observe a variation of more argillaceous mudstones interbedded with variably argillaceous-siliceous (detrital silt-sized quartz rich) and argillaceous-calcareous (containing more abundant calcareous microfossils) mudstones that record stratigraphic variations of different depositional environments within the Balder and Frigg Formations (Figure 6). Some samples are particularly enriched in diagenetic cements, most notably siderite and pyrite.

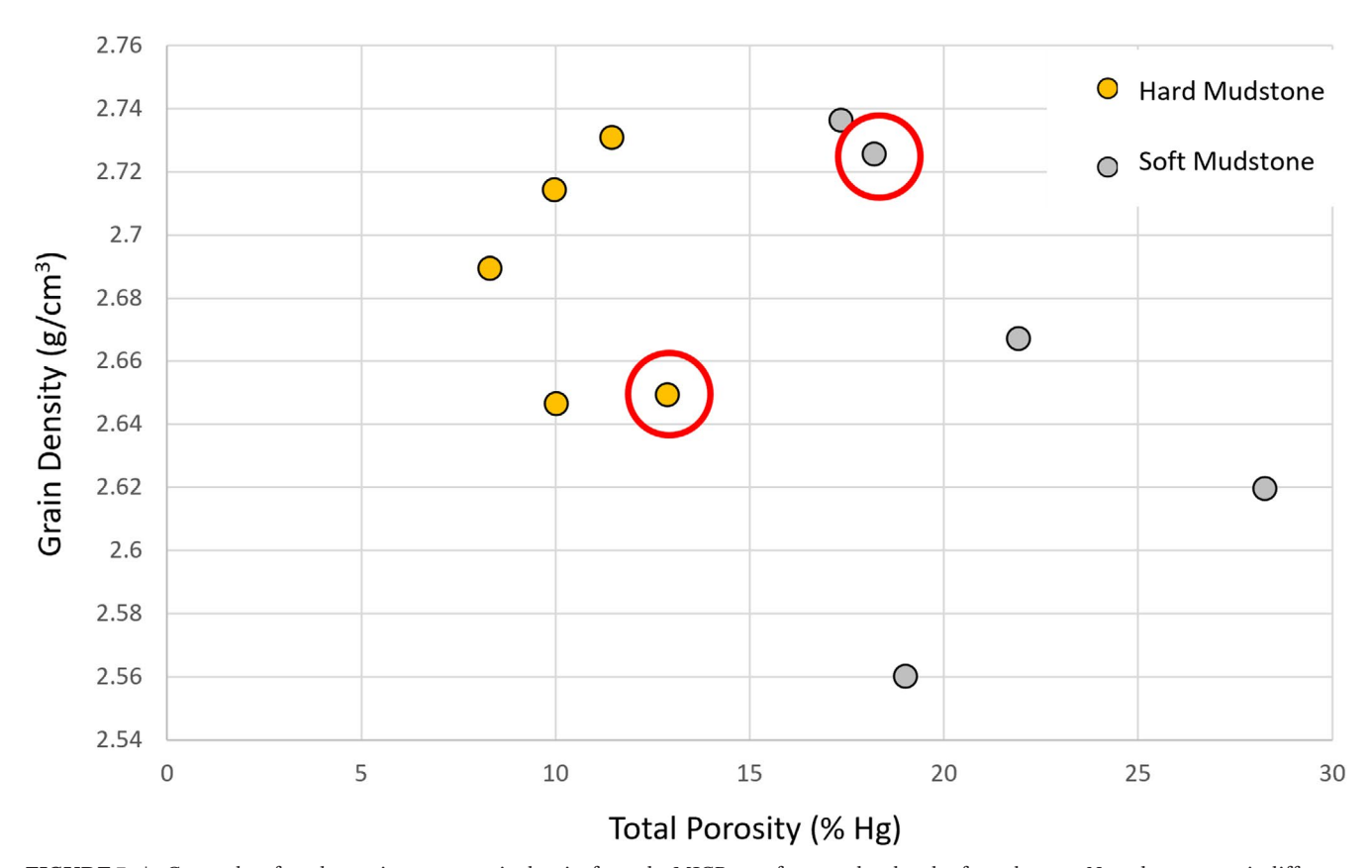


FIGURE 7 | Cross-plot of total porosity versus grain density from the MICP tests for some hard and soft mudstones. Note the systematic difference in total porosity, while there is not a systematic variation in grain density. Highlighted samples are shown in Figure 8.

"Soft" Shale: 9/15-2a; 6355MD, bioturbated calcareous-argillaceous mudstone, grain density 2.67g/cm³, porosity 21.92%



"Hard Shale": 9/19-8; 5406MD, pyrite-bearing calcareous-argillaceous mudstone, grain density 2.65, porosity 12.88%

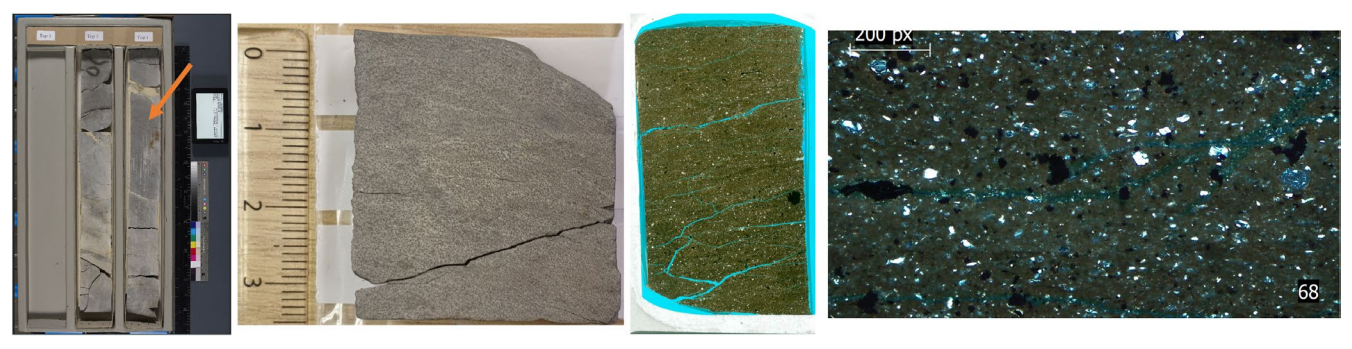


FIGURE 8 | Core, thin-section scan and thin-section micrographs comparing the (micro)texture of a soft and hard mudstone. While both display disrupted fabrics, these fabrics are most likely associated with bioturbation. No obvious deformation fabrics are observed in the hard mudstone, although we may be looking for rather cryptic fabrics associated with deformation of soft mudstone. Top: BGS Sample number SSK144262. Bottom: BGS Sample number SSK144262.

MICP tests were performed on 10 samples; the results show a striking quantifiable bimodal distribution of porosities, without a systematic difference in grain density (Figure 7). At approximately equivalent burial depths (and approximately similar regional effective stress regimes), the porosity reduction in hard mudstone relative to soft mudstone is a factor of two, with an approximate reduction from more than 20% total porosity to 10% (Figure 7).

At the sub-mm thin-section scale, alteration of primary (bedding) fabrics is observed in both soft and hard mudstones, interpreted as polychaeta bioturbation fabrics (Figure 8). No obvious (shear-induced) deformation fabrics are observed in the hard mudstones surrounding injectites.

We can calculate acoustic impedance from the wireline log compressional sonic and bulk density curves for all the wells (dm-scale resolution). Using these calculated curves (Figure 4) we can classify the samples by their occurrence in either hard or soft overall intervals. Using this classification, we observe that broad mineralogical trends within mudstones do not correlate to systematic changes in mudstone impedance (Figure 6). While at the wireline log scale, we do observe variations in impedance behaviour that relate to (stratigraphic and diagenetic) subtle lithofacies changes (Figure 9), the magnitude of that variability is far smaller than the magnitude of acoustic impedance changes associated with hard mudstones around sand injection complexes (compare Figures 4 and 9).

The striking correlation with the wireline log-based impedance classification is observed in the bimodal Hg porosity measurements from the MICP tests (Figure 7), where the samples with

porosities between 8% and 12% are consistently present within sections of high impedance mudstones, whereas the samples with total porosities between 17% and 28% are consistently present within low impedance mudstone intervals.

4 | Regional and Local Seismic Observations

The top Balder Formation is a regionally developed (low) impedance boundary that can be mapped across the Beryl embayment and south Viking Graben (Huuse et al. 2004). The reflector separates more variable (higher) impedance mudstone in the overlying Frigg Formation from lower impedance mudstone in the Balder Formation (Figure 9).

There is a distinct difference in the lithofacies associated with the impedance behaviour of mudstones in the Frigg interval relative to those in the Balder interval. The 'Top Balder' seismic reflector is associated with the interface between the underlying more homogenously argillaceous (and influenced by volcanic ash-derived deposits and its diagenetic alterations) softer Balder mudstones and the overlying mudstones in the Frigg interval that typically contain more abundant detrital silt-sized quartz and which locally are carbonate-cemented, as well as intervals that contain more abundant biogenic calcareous material (Figure 9). The top seismic balder reflector on inverted seismic data is the interface between hard mudstones above and soft mudstones below (Figure 10). Numerous sandstone intrusions are present near the balder seismic reflector and penetrate across the interface. At the resolution of the seismically inverted data, it is sometimes difficult to separate the hard mudstone response around injectites from the

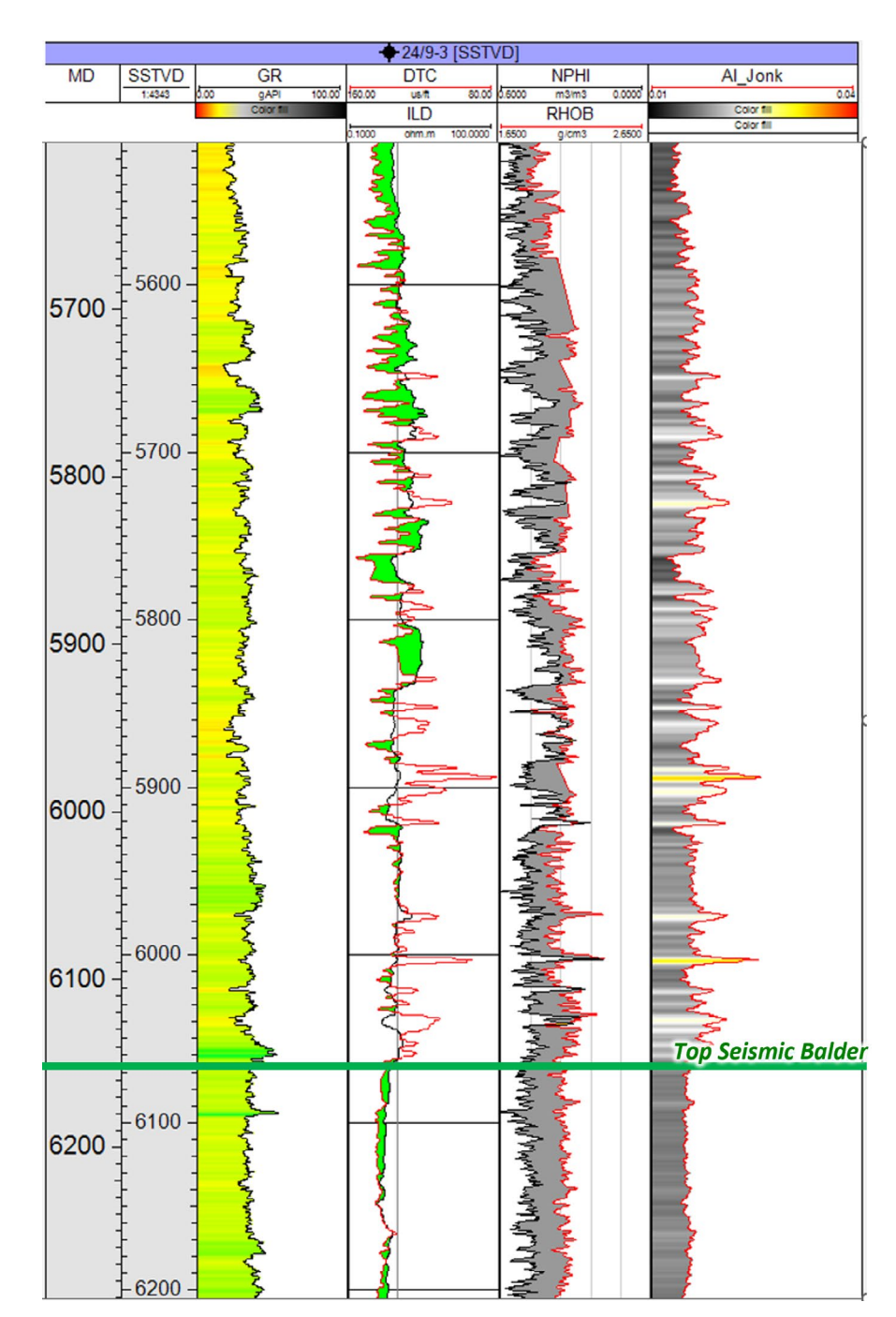


FIGURE 9 | Wireline log display (24/9-3 well) of mudstone across the Balder and Frigg intervals devoid of sandstone intrusions, displaying stratigraphically and diagenetically driven impedance variations within mudstones. Compare the magnitude of impedance variations (on the same scale) to what is observed around injectites in the display in Figure 4. Note the presence of the Top Balder seismic reflector, which corresponds to a change to siltier mudstones above to (lower impedance) argillaceous mudstones below the reflector. The Balder Seismic reflector is associated with a decrease of acoustic impedance.

impedance event associated with the top balder reflector when both are present in the same zone (Figure 10).

When mapping specific examples of injectites in close proximity to the seismic balder reflector, we can pick out a correlation of wireline log-based hard mudstones associated with injectites, and a tuned seismic response associated with the hard shoulders around the injectites when considering reflectivity data where calibration data from well logs is present. In some

cases, at the resolution of the seismic data, a single tuned high impedance inverted interval is observed, where the sandstone intrusions are thinner than the broader high impedance mudstone encompassing the sand injection complex (Figure 11A). In other cases, the sandstone intrusion complex is developed to a thickness where we observe a low impedance (sand-dominated) centre surrounded by high impedance mudstones in the inverted seismic data, calibrated against impedance curves from the wireline logs (Figure 11B). In areas where the

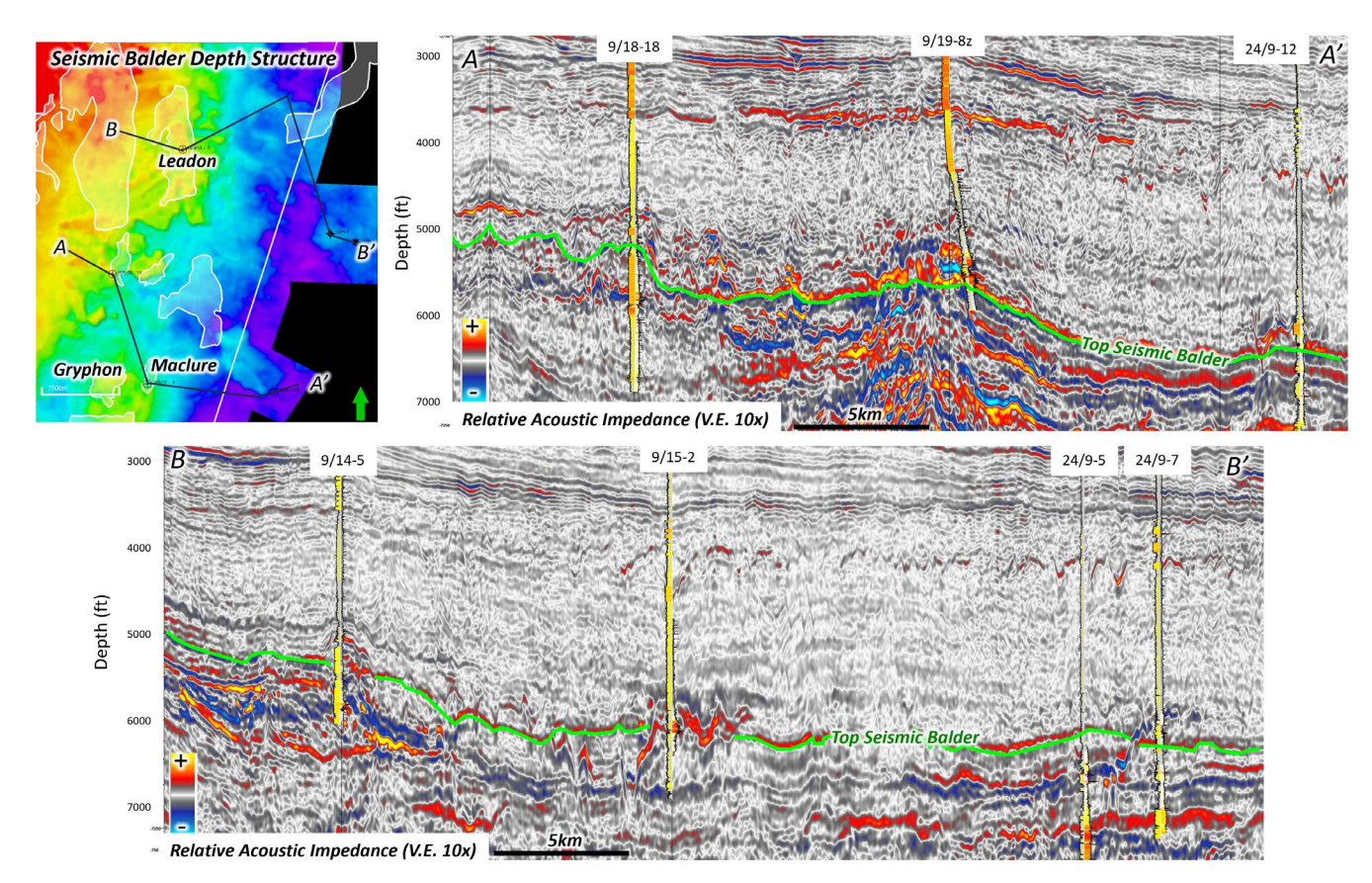


FIGURE 10 | Regional seismic sections of inverted relative acoustic impedance showing the broad seismic expression of the Frigg-Balder interface (top Balder reflector in green) on the inverted seismic data relative to some of the key wells associated with sand injection complexes that are located close to the Balder-Frigg seismic-stratigraphic interface wells show GR (left) and acoustic impedance (right) logs with the same display parameters as used in the well log displays (Figure 4).

sand injection complex is dominated by steeply-dipping (dykedominated) intrusions, the imaging and associated inversion can be more problematic (Figure 11C) and the wireline log observations may be more difficult to calibrate appropriately against a seismic response. Generally, the observed high impedance boundaries around certain sand injection complexes resolved from the seismically inverted data are of high fidelity, given the strong calibration to the wireline log response in places (Figure 11). As such, we can generally use the inverted angle stack reflectivity data to identify potential areas of complex seismic responses within injectite reservoirs that require more scrutiny when considering the AVO-based responses in the context of reservoir fluid type.

5 | Discussion

5.1 | The Origin of High Impedance Mudstone Around Sand Injection Complexes

Systematic correlation of mineralogical variability with acoustic impedance may support the likelihood of models 1 or 2 (preferential sill-like intrusion along mechanical stratigraphic variability or preferential cementation along injectite margins respectively) as the favoured scenarios for explaining anomalous high impedance mudstones associated with sandstone injection complexes

(Figure 5). However, there is no systematic correlation between mineralogy represented by the bulk chemistry XRF data and the impedance of the mudstones (Figure 6). Second-order impedance variability is observed and related to stratigraphic and diagenetic processes (Figure 9). The magnitude of these variations is dwarfed by the impedance variations observed around large sand injection complexes (Figure 4).

Mudstone impedance correlates strongly with total porosity, as is observed in the MICP data (Figure 7). The porosity reduction does not correlate with anomalous cementation or textural relationships of different lithofacies. Rather, porosity reduction is associated with sediment mechanical compaction. This can be explained by both simple shear (shear-induced deformation in mudstones during injection, model 3) or pure shear (mechanical compaction due to anomalous dewatering of mudstone around permeable injected sandstone, model 4) effective stress-induced compaction (Figure 5).

No obviously abundant deformation fabrics are observed in the mudstones, either at core or thin-section scale (Figure 8). This does not preclude the possibility of model 3 (Figure 5) as a causal mechanism, as deformation fabrics induced in mudstones during injection may be subtly preserved and observed (Ibanez and Kronenberg 1993). Some minor brittle deformation fabrics are present, but are typically only present within a few centimetres

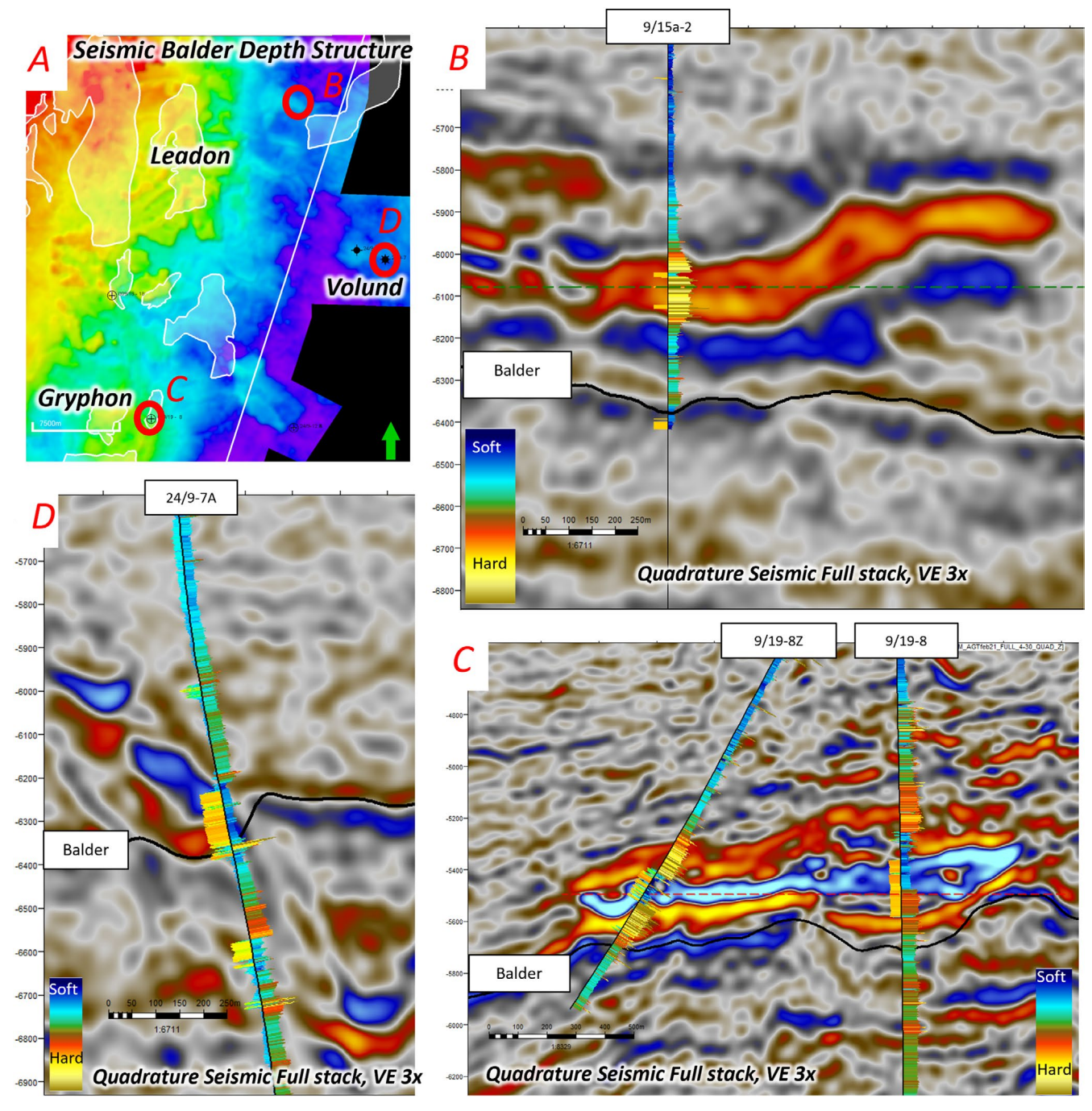


FIGURE 11 | Examples of wireline log-calibrated seismic full stack responses of hard and soft mudstone around specific sand injection complexes. (A) Balder Depth Structure map showing the location of the specific well-seismic calibration displays. (B): A sill-dominated response calibrated to the 9/15-2 well. (C) Sill-dominated response associated with the Maclure field calibrated to wells 9/19-8 and 9/19-8Z. (D) A muted response associated with a dyke-dominated response around the 24/9-7 well in the Volund field. Note the presence of hardening mudstone associated with the deeper sand, but a more muted mudstone response associated with the shallower sand.

of the injectite margins (Hurst et al. 2025) and would not generate the broad high impedance zonation observed in wireline log and seismic data.

The most likely cause of the high impedance hardening of mudstone around injectite complexes is associated with a pure shear volume reduction of porosity. This would be associated with locally increased effective stress, most likely caused by reduction of pore fluid pressure. Focused dewatering of mudstone into surrounding permeable sandstone intrusions that connect volumes of higher pore pressure with volumes of lower pore pressure would be the most likely candidate to dissipate fluid pressure fast and cause local anomalous pore pressure reduction in mudstones. Sand injectites can provide long-lived flow conduits through low permeability strata (Jonk, Parnell, and Hurst 2005; Cartwright et al. 2007; Jonk 2010) and appear

to be dynamically acting as conduits for aqueous fluid flow in an actively dewatering sedimentary basin with a recent Tertiary mudstone-dominated sediment load (Moss et al. 2003; Robertson et al. 2013).

5.2 | Implications for Regional Pore Pressure Distribution and Fluid Retention and Escape

Regional observations of the onset of primary overpressure generation across the Frigg-Balder interface coincide approximately with the slope-to-basin-floor transition of the overlying Frigg and Hordaland formations, consisting of thick mudstone-dominated sequences interpreted to cause the onset of primary overpressure (disequilibrium compaction) above the submud depth interval of about 1600 to 1800 m burial (5500–6000ft) in the basin (Moss et al. 2003), which coincides with the approximate burial depth for the majority of the sandstone injection complexes in the overpressured part of the basin at present day (Figure 12).

This may explain why the high impedance mudstones around the Balder-Frigg stratigraphic interval are predominantly observed to the east of the slope-to-basin floor transition (Figure 12),

and only at burial depths greater than approximately 1600 to 1800 m below mudline. In more detail, the distribution of high impedance mudstones associated with dynamic dewatering is more complex and follows the principle of a centroid configuration of dewatering and associated pressure variations (Bruce and Bowers 2002; Mourgues et al. 2011). The centroid concept (sometimes referred to as lateral pressure transfer; Yardley and Swarbrick 2000) considers a dipping permeable (sandstone) body encased within mudstones, with lower mudstone overpressure at the top of the sandstone relative to the mudstones at the base of the sandstone. In this configuration, the fluid pressure at the 'mid-point' of the sandstone body is expected to be at the same pressure as immediately adjacent mudstones. Given the permeability of the sandstone, fluid pressure in the sandstone would follow a hydrostatic gradient. As such, at the base of the dipping reservoir, mudstone fluid pressure would exceed the fluid pressure in the sandstone, whereas at the top of the dipping reservoir, the reverse would be true. In that setting, mudstones towards the base would dewater into the sand (towards lower fluid pressure), whereas mudstones towards the top of the dipping reservoir would be expected to receive expelling fluids from the reservoir and therefore generate additional overpressure (Figure 13A).

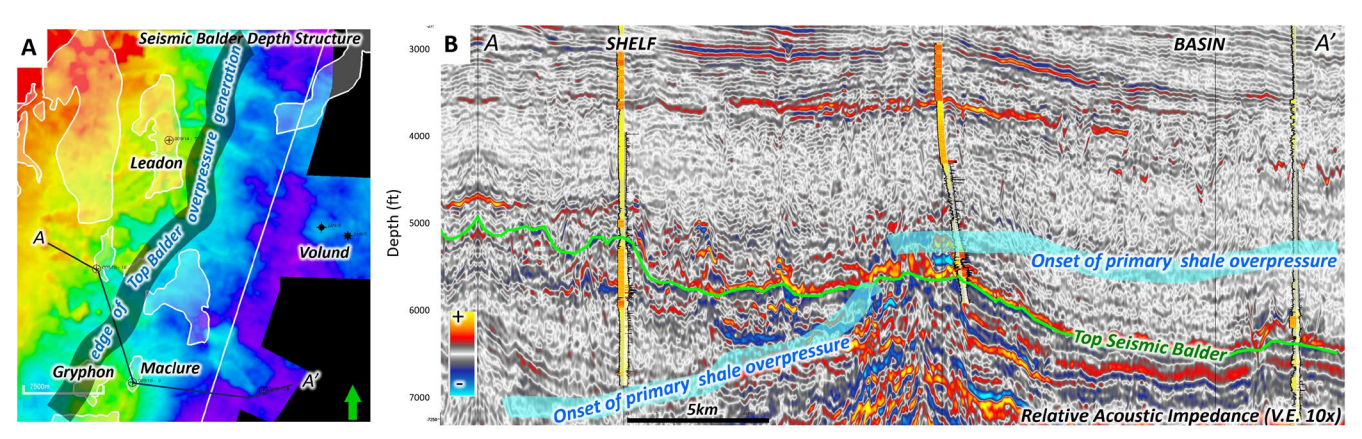


FIGURE 12 | Map (A) and seismic section (B) showing the approximate onset of primary overpressure generation across the Balder surface. Note the distinct change of the depth of overpressure from the shelfal to the basinal region corresponding broadly to the underlying margin of the East Shetland platform bounding fault (Figure 3).

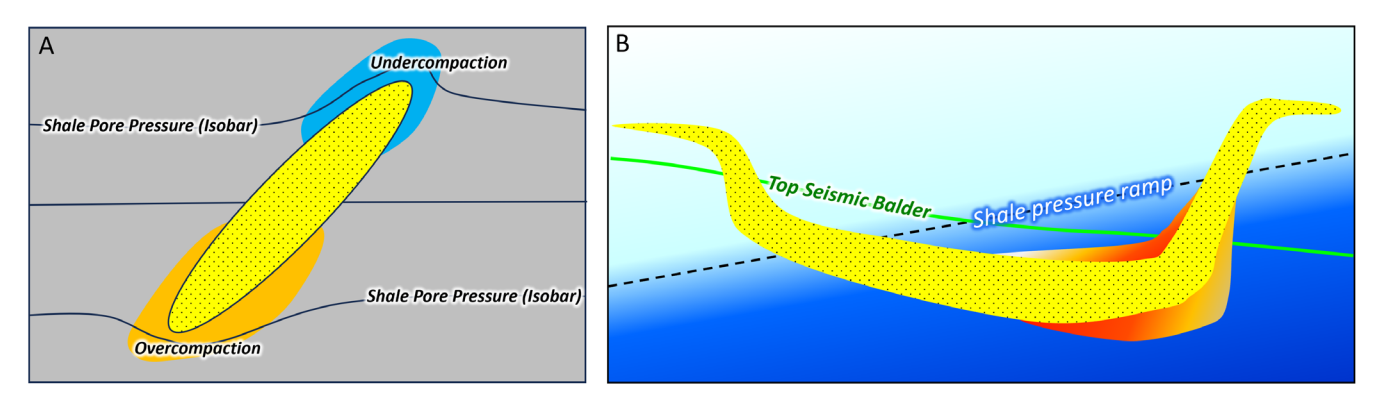


FIGURE 13 | (A) The centroid concept associated with fluid pressure changes (and associated mudstone under and over compaction) because of mudstone dewatering through permeable vertically connected sandstone. (B) The centroid concept applies to sand injectites that connect across primary overpressure zones in the mudstone. The flow of water from high pressure zones to low pressure zones leads to the development of hard (overcompacted) mudstones in the regions of most severe pressure gradient change associated with the adjacent permeable sand injectites (indicated with the red shaded region).

In this model, the expectation is that anomalously high impedance mudstones are associated not only with large injectite complexes in primary (aqueous) overpressured settings, but the distribution of hard (dewatered) mudstones is likely to be focused around the most overpressured (deeper) parts of injectite complexes, where dewatering is facilitated by the permeable injectites, causing increased effective stress and thus mechanical compaction. The hard mudstones would be most accentuated along the basal parts of large vertically oriented injectites (dykes) that connect the overpressured regions to regions approaching hydrostatic pressures (Figure 13A). This leads to a more complex three-dimensional structure of hard mudstones around injectite complexes, and the presence, absence and magnitude of mudstone hardening observed in wells will be variable as a function of the exact location of the well relative to the geometry of the injectite complex and the regional aqueous primary pressure ramp (Figure 13B). This model is a simplification of the complex dynamic behaviour of fluid flow and associated effective-stress induced compaction, and with (geologic) time and continued burial, the behaviour would be expected to alter dynamically. Given the complex geometries of sandstone injection complexes and the complex (dynamic) changing permeability structure of the complex and the surrounding mudstones, the ability to map seismic attributes to rock properties (such as lithology and porosity) and ultimately fluid type predictions from seismic attributes is complex and not necessarily intuitive.

6 | Conclusions

High impedance (hard) mudstone associated with sand injection complexes causes complexities when evaluating AVObased attributes for reservoir fluid prediction. It is important to understand the processes by which these high impedance mudstones form, to enable more confident calibration of fluid predictions. Within the Balder and Frigg formations in the Beryl Embayment and South Viking Graben, hard mudstones are not ubiquitous, but rather associated with large-scale injectite complexes in the slope-to-basin-floor transition hosted by the Balder and Frigg Formations. Rock physical and thinsection observations on core samples from high and low impedance mudstones adjacent to sandstone intrusions show that high impedance is associated with mechanical compaction and a porosity reduction of a factor of 2 is observed within hard mudstones when compared to the more typical low impedance mudstones. We interpret this porosity reduction to be caused by locally increased effective stress associated with dewatering of overpressured mudstone into permeable sand injectites that vertically connect to regions of lower pressure, much akin to the centroid concept more widely developed for large-scale sand bodies that connect across mudstone pore pressure regimes. High impedance mudstone is likely to occur within the (basal) portions of injectite complexes which vertically connect through a primary overpressure transition. Within overpressured sedimentary basins, lateral transfer is an efficient and dominant mode of fluid escape (Yardley and Swarbrick 2000; Osborne and Swarbrick 1997). This process is often associated with extensive dipping aquifers and/or large fault conduits. Sandstone injection complexes may provide an additional (previously overlooked) mode of efficient lateral fluid transfer in overpressured basins.

Acknowledgements

This work was performed as part of Bader Al-Aamri's M.Sc. project at the University of Aberdeen in 2022. We thank Andrew Hurst and Matt Brettle for their support in the project. We thank PGS for permission to show the seismic data in Figures 10 and 11. We thank Apache management and Harbour management for their support in publishing this work. We also thank the British Geological Survey for providing the subsampled core material, Loan Number: 286254, and the UKCS (offshore) hydrocarbon wells database for providing an open access portal to offshore core photographs. We thank Andrew Hurst, Nicholas Satur, and an anonymous reviewer for thoughtful reviews that helped improve the manuscript.

Conflicts of Interest

The authors declare no conflicts of interest.

Data Availability Statement

The data that support the findings of this study are available from the corresponding author upon reasonable request.

Peer Review

The peer review history for this article is available at https://www.webof science.com/api/gateway/wos/peer-review/10.1111/bre.70058.

References

Ahmadi, Z. M., M. Sawyers, S. Kenyon-Roberts, et al. 2003. "Paleocene." In *The Millennium Atlas: Petroleum Geology of the Central and Northern North Sea*, edited by D. Evans, C. Graham, A. Armour, and P. Bathurst, 235–259. Geological Society of London.

Bruce, B., and G. Bowers. 2002. "Pore Pressure Terminology." $Leading\ Edge\ 21,\ no.\ 2:\ 170-173.$

Cartwright, J., M. Huuse, and A. Aplin. 2007. "Seal Bypass Systems." *AAPG Bulletin* 91, no. 8: 1141–1166.

Cartwright, J., D. James, M. Huuse, W. Vetel, and A. Hurst. 2008. "The Geometry and Emplacement of Conical Sandstone Intrusions." *Journal of Structural Geology* 30, no. 7: 854–867.

Castagna, J. P., H. W. Swan, and D. J. Foster. 1998. "Framework for AVO Gradient and Intercept Interpretation." *Geophysics* 63, no. 3: 948–956.

Davudov, D., R. G. Moghanloo, and Y. Lan. 2018. "Evaluation of Accessible Porosity Using Mercury Injection Capillary Pressure Data in Mudstone Samples." *Energy & Fuels* 32, no. 4: 4682–4694.

Hou, X., Y. He, and B. T. Jones. 2004. "Recent Advances in Portable X-Ray Fluorescence Spectrometry." *Applied Spectroscopy Reviews* 39, no. 1: 1–25.

Hurst, A., J. Cartwright, M. Huuse, et al. 2003. "Significance of Large-Scale Sand Injectites as Long-Term Fluid Conduits: Evidence From Seismic Data." *Geofluids* 3, no. 4: 263–274.

Hurst, A., R. van Oorschot, A. Grippa, and G. Palladino. 2025. "Identification of Sand Injectite Facies in Core: Their Significance to Developing a Reservoir Model for the Chestnut Oilfield, UK Continental Shelf." In *Geological Society, London, Energy Geoscience Conference Series*, vol. 1, No. 1, pp. egc1-2024. Geological Society of London.

Huuse, M., D. Duranti, N. Steinsland, et al. 2004. "Seismic Characteristics of Large-Scale Sandstone Intrusions in the Paleogene of the South Viking Graben, UK and Norwegian North Sea." *Geological Society, London, Memoirs* 29: 263–278.

Ibanez, W. D., and A. K. Kronenberg. 1993. "Experimental Deformation of Shale: Mechanical Properties and Microstructural Indicators of

Mechanisms." International Journal of Rock Mechanics and Mining Sciences & Geomechanics Abstracts 30, no. 7: 723–734.

Jones, E., R. Jones, C. Ebdon, et al. 2003. "Eocene." In *The Millennium Atlas: Petroleum Geology of the Central and Northern North Sea*, edited by D. Evans, C. Graham, A. Armour, and P. Bathurst, 261–277. Geological Society of London.

Jonk, R. 2010. "Sand-Rich Injectites in the Context of Short-Lived and Long-Lived Fluid Flow." *Basin Research* 22, no. 4: 603–621.

Jonk, R., K. M. Bohacs, and J. S. Davis. 2022. "Evaluating Top Seals Within a Sequence-Stratigraphic Framework: Impact on Geological Carbon Sequestration." *Marine and Petroleum Geology* 146: 105920.

Jonk, R., D. Duranti, J. Parnell, A. Hurst, and A. E. Fallick. 2003. "The Structural and Diagenetic Evolution of Injected Sandstones: Examples From the Kimmeridgian of NE Scotland." *Journal of the Geological Society* 160, no. 6: 881–894.

Jonk, R., A. Hurst, D. Duranti, J. Parnell, A. Mazzini, and A. E. Fallick. 2005. "Origin and Timing of Sand Injection, Petroleum Migration, and Diagenesis in Tertiary Reservoirs, South Viking Graben, North Sea." *AAPG Bulletin* 89, no. 3: 329–357.

Jonk, R., J. Parnell, and A. Hurst. 2005. "Aqueous and Petroleum Fluid Flow Associated With Sand Injectites." *Basin Research* 17, no. 2: 241–257.

Milliken, K. 2014. "A Compositional Classification for Grain Assemblages in Fine-Grained Sediments and Sedimentary Rocks." *Journal of Sedimentary Research* 84, no. 12: 1185–1199.

Moss, B., D. Barson, K. Rakhit, H. Dennis, and R. Swarbrick. 2003. "Formation Pore Pressures and Formation Waters." In *The Millennium Atlas: Petroleum Geology of the Central and Northern North Sea*, edited by D. Evans, C. Graham, A. Armour, and P. Bathurst, 317–329. Geological Society of London.

Mourgues, R., J. B. Gressier, L. Bodet, D. Bureau, and A. Gay. 2011. ""Basin Scale" Versus "Localized" Pore Pressure/Stress Coupling–Implications for Trap Integrity Evaluation." *Marine and Petroleum Geology* 28, no. 5: 1111–1121.

Osborne, M. J., and R. E. Swarbrick. 1997. "Mechanisms for Generating Overpressure in Sedimentary Basins: A Reevaluation." *AAPG Bulletin* 81, no. 6: 1023–1041.

Pernin, N., L. Feuilleaubois, T. Bird, and C. Reiser. 2022. "Identifying and De-Risking Near-Field Opportunities Through Reliable Pre-Stack Broadband Attributes: Examples From the Paleocene North Sea (UK-Norway) Injectites Play." In *Cross-Border Themes in Petroleum Geology I: The North Sea*, edited by S. Patruno, S. G. Archer, D. Chiarella, J. A. Howell, C. A.-L. Jackson, and H. Kombrink. Geological Society London Special Publications.

Purvis, K., J. Kao, K. Flanagan, J. Henderson, and D. Duranti. 2002. "Complex Reservoir Geometries in a Deep Water Clastic Sequence, Gryphon Field, UKCS: Injection Structures, Geological Modelling and Reservoir Simulation." *Marine and Petroleum Geology* 19, no. 2: 161–179.

Robertson, J., N. R. Goulty, and R. E. Swarbrick. 2013. "Overpressure Distributions in Palaeogene Reservoirs of the UK Central North Sea and Implications for Lateral and Vertical Fluid Flow." *Petroleum Geoscience* 19, no. 3: 223–236.

Satur, N., and A. Hurst. 2025. "The Value of Outcrops in Understanding the Complexities of Sand Intrusion Reservoirs: Learnings From the Volund Field." *Basin Research* 37, no. 2: e70025.

Simm, R. 2017. "A 'Sense Check' Method for Incorporating Seismic Amplitude Information Into Prospect Risk (a Tribute to Mike Bacon)." *First Break* 35, no. 10: 45–49.

Szarawarska, E., M. Huuse, A. Hurst, et al. 2010. "Three-Dimensional Seismic Characterisation of Large-Scale Sandstone Intrusions in the Lower Palaeogene of the North Sea: Completely Injected vs. In Situ Remobilised Sandbodies." *Basin Research* 22, no. 4: 517–532.

Templeton, G., P. T. King, and M. L. Reeder. 2002. "Leadon Field-Description of Frigg Reservoir Sand Injection Structures." In *64th EAGE Conference & Exhibition* (pp. cp-5). European Association of Geoscientists & Engineers.

Vigorito, M., and A. Hurst. 2010. "Regional Sand Injectite Architecture as a Record of Pore-Pressure Evolution and Sand Redistribution in the Shallow Crust: Insights From the Panoche Giant Injection Complex, California." *Journal of the Geological Society* 167, no. 5: 889–904.

Vigorito, M., A. Hurst, A. J. Scott, O. Stanzione, and A. Grippa. 2022. "A Giant Sand Injection Complex: Processes and Implications for Basin Evolution and Subsurface Fluid Flow." *American Journal of Science* 322, no. 6: 729–794.

Waltham, R. J., G. Zvirtes, B. S. Burnham, and A. Hurst. 2025. "Geometric and Spatial Analysis of Wing-Like Intrusions as Outcrop Analogues for Subsurface Analysis." *Basin Research* 37, no. 3: e70036.

Yardley, G. S., and R. E. Swarbrick. 2000. "Lateral Transfer: A Source of Additional Overpressure?" *Marine and Petroleum Geology* 17, no. 4: 523–537.